ACS Catalysis

Research Article

pubs.acs.org/acscatalysis

Size-Dependent Catalytic Performance of CuO on γ-Al_2O_3: NO Reduction versus NH_3 Oxidation

Ja Hun Kwak,*[,†] Russell Tonkyn,[†] Diana Tran,[†] Donghai Mei,*[,†] Sung June Cho,[‡] Libor Kovarik,[†] Jong H. Lee,[†] Charles H. F. Peden,[†] and János Szanyi[†]

[†]Institute for Integrated Catalysis, Pacific Northwest National Laboratory, Richland, Washington 99352, United States

[‡]Department of Applied Chemical Engineering, Chonnam National University, Korea

Supporting Information

ABSTRACT: Catalytic reaction pathways of NH_3 on CuO/γ-Al_2O_3 catalysts during NH_3 selective catalytic reduction reactions were investigated under oxygen-rich conditions. On 10 wt % CuO/γ-Al_2O_3, NH_3 reacted with oxygen to produce NO_x. In contrast, on the 0.5 wt % CuO/γ-Al_2O_3 catalyst, NH_3 reacted primarily with NO to form N_2 with a conversion efficiency of ~80% at 450 °C. H_2-temperature-programmed reduction (H_2-TPR) results show that Cu species present in 10 wt % CuO/γ-Al_2O_3 can be easily reduced at ~160 °C, which suggests the formation of large CuO clusters on the alumina surface. On the other hand, the TPR spectrum obtained from the 0.5 wt % CuO/γ-Al_2O_3 catalyst does not show any measurable H_2 consumption up to 700 °C, which suggests the presence of nonreducible isolated Cu species in this catalyst. Scanning transmission electron microscopy images collected from 10 wt % CuO/γ-Al_2O_3 show nanosized CuO clusters, but no evidence of cluster formation is seen in the images recorded from the 0.5 wt % CuO/γ-Al_2O_3 sample due to the intrinsic limitation of low Z contrast between highly dispersed Cu (atomic weight = 63.5) species and the alumina support (atomic weight of Al = 27). EXAFS data indicates the presence of Cu−Cu (Al) second shell at 0.35 nm only in the 10 wt % CuO/γ-Al_2O_3 catalyst, and an estimated coordination number of ~1.7. The XANES and EXAFS results suggest the formation of relatively highly dispersed Cu oxide nanoclusters, even at 10 wt % Cu loading. Density functional theory results show that supported CuO clusters, represented by a two-dimensional CuO monolayer, can effectively dissociate adsorbed NO and O_2 to produce atomic oxygen species. These reactive atomic oxygen species then react with NH_3 to produce NO_x. However, the nonreducible, isolated Cu species, modeled by γ-Al_2O_3-supported monomeric CuO, shows relatively weak interactions with both NO and O_2. Most importantly, our calculations suggest that the dissociations of either NO or O_2 are energetically unfavored on this latter catalyst. Therefore, molecularly adsorbed NO can react only with NH_3 to produce N_2 on the low (0.5 wt %) CuO-loaded catalyst.

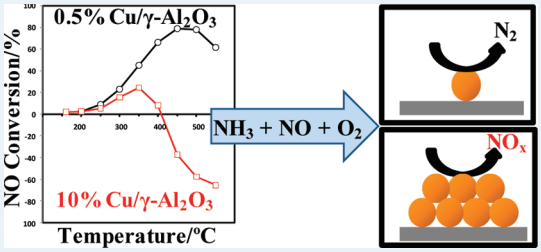

KEYWORDS: *selective catalytic reduction, γ-alumina, copper oxide, ammonia, nitric oxides, morphological effects, density functional theory*

1. INTRODUCTION

Establishing structure-performance relationships in heterogeneous catalysis has long been of great interest in both fundamental and applied research.[1,2] Despite this longstanding interest, limitations of suitable analytical tools to study subnanometer-sized catalyst structures (the scale of most catalytic phases on high surface area supports) hindered many of these efforts. The remarkable recent advances in catalyst characterization methods combined with novel synthetic approaches is providing significantly enhanced molecular level understanding of both the structure of supported catalytic phases and their catalytic properties.[3,4] These new approaches are profoundly effecting the development of new catalysts with specific and sometimes previously unknown catalytic properties. For example, Chen and Goodman have reported that Au clusters (2−3 nm) supported on titanium dioxide exhibited very high CO oxidation activity, contradicting the longstanding belief that Au was catalytically inert.[5] Recently, Vajda and co-workers have also shown that subnanometer-sized Ag clusters supported on alumina can efficiently catalyze the direct epoxidation of propylene, especially when Ag clusters were primarily deposited as trimers.[6]

Although these recent efforts have realized considerable success for the control of catalyst morphologies and consequently the tailoring of catalytic properties, structure−property relationships in most practical catalyst systems are not adequately understood. This is particularly the case in catalyst systems where the most active component may be monoatomically dispersed. In these systems, difficulties arise both from the

Received: October 27, 2011
Revised: May 24, 2012
Published: May 25, 2012

   dx.doi.org/10.1021/cs3002463 | ACS Catal. 2012, 2, 1432−1440

preparation and the characterization of such atomically dispersed active phases.

Recently, we reported combined ultrahigh magnetic field solid state ^{27}Al NMR and high-resolution scanning transmission electron microscopy (STEM) studies that clearly showed the role of the pentacoordinate aluminum sites, formed on the (100) facets of γ-Al_2O_3, as the preferential anchoring points for catalytically active phases, such as BaO and Pt.[7−9] Furthermore, high-resolution STEM images have shown that active oxides and metals were "monoatomically" dispersed on the (100) facets of γ-Al_2O_3. These results have clearly suggested a strong interaction between catalytic phases and special surface sites that, in turn, can be utilized for the preparation of highly dispersed and thermally stable γ-Al_2O_3-supported catalysts that may also exhibit unique catalytic properties.

In this contribution, we report on the vastly different catalytic properties of monoatomically dispersed and large Cu clusters supported on γ-Al_2O_3 during NO_x reduction by NH_3 in excess O_2. For relatively large clusters of CuO, NH_3 reacts primarily with oxygen and produces NO_x. In contrast, NH_3 selectively reacts with NO_x to produce N_2 on isolated Cu sites on the alumina support, even under highly oxidizing conditions. The present work indicates that the catalytic reaction pathways can be controlled by tuning the size of the active metal clusters on alumina. Most importantly, the catalytic behavior of monomeric CuO supported on alumina studied here provides a unique insight into the single-atom catalyzed reaction, which may play an important role in the overall selective catalytic reduction (SCR) activity observed over hydrothermally aged Cu-zeolite catalysts.

2. EXPERIMENTAL AND COMPUTATIONAL PROCEDURES

CuO/γ-Al_2O_3 catalysts with varying Cu loadings were prepared on a commercial γ-Al_2O_3 powder (Condea, BET surface area = 200 m^2/g) by the incipient wetness method using $Cu(NO_3)_2$ as the precursor. After drying in air at 373 K for 15 h, the samples were calcined at 773 K in flowing dry air for 2 h.

All reactivity measurements were conducted in a packed-bed microreactor system using 100 mg of catalyst powder samples. The reaction temperature was measured by a thermocouple placed inside the catalyst bed. Unless specified otherwise, the activity was measured using a feed gas mixture containing 350 ppm NO, 350 ppm NH_3, 14% O_2, 2% H_2O, and the balance N_2, and the total flow rate was held at 300 sccm. The concentrations of all reactant and product species were measured using a Nicolet Magna 760 infrared spectrometer (FT-IR) equipped with a heated 2-m path length gas cell. The catalysts were evaluated for their activity toward NO reduction and NH_3 oxidation (performed in the absence of NO) reactions. The percentages of NO and NH_3 conversions were calculated on the basis of the differences in their concentrations measured before and after the catalyst bed.

$$\text{NO conversion \%} = \{\text{NO}_{\text{inlet}} - (\text{NO} + \text{NO}_2 + 2\text{N}_2\text{O})_{\text{outlet}}\} / \text{NO}_{\text{inlet}} \times 100$$

$$\text{NH}_3\ \text{conversion \%} = (\text{NH}_{3,\text{inlet}} - \text{NH}_{3,\text{outlet}})/\text{NH}_{3,\text{inlet}} \times 100$$

Prior to H_2-TPR (temperature-programmed reduction) experiments, 0.05 g of each CuO/γ-Al_2O_3 catalyst was calcined at 500 °C for 2 h under air flow (1.0 mL/s). After calcination, the sample was cooled to room temperature (RT) under air flow and then purged with 2% H_2/Ar (1.0 mL/s) for 1 h at RT. After stabilization of the thermal conductivity detector (TCD) signal of the Hewlett-Packard 7820 gas chromatograph (GC), a TPR experiment was carried out in 2% H_2/Ar (1.0 mL/s) flow with a heating rate of 10 K/min. H_2 consumption was determined from the TCD signal intensities calibrated using TPR spectrum of 10 wt % CuO/SiO_2.

High-resolution TEM imaging was performed with an FEI Titan 80-300 microscope operated at 300 kV. The instrument is equipped with a CEOS GmbH double-hexapole aberration corrector for the probe-forming lens, which allows imaging with 0.1 nm resolution in STEM mode. The images were acquired in high angle annular dark field with an inner collection angle of 52 mrad. The sample preparation for the TEM measurements involved mounting of the Cu-loaded γ-Al_2O_3 powder on lacey carbon TEM grids and immediate loading into the TEM airlock to minimize extended exposure to atmospheric O_2.

The EXAFS data were collected at the National Synchrotron Light Source on beamline 18B operating at 2.8 GeV. The ring current was maintained at ~300 mA, and a Si(111) channel cut monochromator was used. All the samples were calcined at 500 °C for 2 h in air and then pasted onto Kapton tape in a glovebox (<0.1 ppm H_2O and O_2) to prevent the adsorption of H_2O. EXAFS data were taken at room temperature by using a passivated implanted planar silicon detector at Cu K edge (8979 eV). To ensure a good signal-to-noise ratio of the EXAFS data, each sample was scanned at least three times.

EXAFS spectra, measured from samples precalcined at 500 °C for 2 h under air flowing conditions, were analyzed using the IFEFFIT package that includes Athena and Artemis. The threshold energy, E_0, for all spectra was taken as the first inflection point in the absorption edge region. A background of raw X-ray absorption data was removed using a new method proposed by Newville et al.[10,11] The low r component in the Fourier transform of the XAFS spectrum was minimized by comparing it with either a theoretical standard from the *Feff6* code or an experimental standard that contained a correct background. After background removal, EXAFS oscillations were normalized using an edge jump and then were weighted by k^3. The $k^3\chi(k)$ data in the range of 20−150 nm^{-1} was Fourier transformed into r space for the curve fit. The theoretical *Feff6* standards were utilized in the curve-fitting routine FEFFIT. During the curve-fitting in q-space after the inverse Fourier transformation, the overall many-body reduction factor, S_0^2, was fixed to 0.8 for all samples. Backscattering amplitudes and phase shifts were calculated using *Feff6* for CuO and $CuAl_2O_4$, respectively.

Density functional theory (DFT) calculations with spin-polarization were performed using the Vienna ab initio simulation package (VASP).[12−14] Core and valence electrons were represented by the projector augmented wave method and plane wave functions with a kinetic energy cutoff of 400 eV.[15,16] The generalized gradient approximation combined with the Perdew−Burke−Ernzerhof functional[17] was used in the calculations. Ground-state atomic geometries were obtained by minimizing the forces on each atom to below 0.05 eV/Å. For the adsorbed systems, all atoms of the adsorbates and the top two atomic layers were allowed to relax while other atoms in the model surface slabs were fixed during optimization. The

dx.doi.org/10.1021/cs3002463 | ACS Catal. 2012, 2, 1432−1440

(2 × 2 × 1) *k*-point sampling scheme was used in these calculations to provide sufficient accuracy.

The transition states of NO and O_2 dissociation were calculated using the nudged elastic band method and its improvements.[18−20] We used eight intermediate images along the reaction path between the initial and final states. The transition states identified were further confirmed as being first-order saddle points using a finite-difference normal-mode analysis. Only one imaginary frequency was obtained at the transition state.

3. RESULT AND DISCUSSION

3.1. Catalytic Activity Tests: NH_3 SCR versus NH_3 Oxidation. During SCR of NO by NH_3, there are two major competing reactions that take place over the catalyst, and their contributions to the overall reaction depend on the catalyst itself and the temperature of the catalyst bed. In general, the overall reaction is dominated by the reduction of NO by NH_3 to form N_2 at low to moderate temperatures. But as the reaction temperature increases, the oxidation of NH_3 by O_2 can become dominant, limiting the availability of NH_3 for NO reduction.

Figure 1a shows the NO conversion during SCR reaction as a function of catalyst bed temperature over 0.5 wt % and 10 wt % CuO/γ-Al_2O_3 samples. Over both catalysts, the NO reduction activity increased initially with increasing temperature, then reached a maximum and decreased at high temperatures. However, the temperature regime of increasing NO reduction activity for these two catalysts are vastly different: NO conversion on the 0.5 wt % CuO/γ-Al_2O_3 sample increases up to 450 °C, whereas the 10 wt % CuO/γ-Al_2O_3 catalyst exhibits the highest NO conversion at 350 °C.

The temperature of maximum NO conversion is not the only difference between the reactivity profiles of these two samples. More important is the level of maximum NO reduction that these two catalysts exhibit: it reaches 80% for the 0.5 wt % sample, but it is lower than 30% on the 10 wt % CuO/γ-Al_2O_3 catalyst. After maximizing at 450 °C, the NO reduction activity for the 0.5 wt % CuO/γ-Al_2O_3 catalyst remains unchanged up to 500 °C before it begins to drop. In contrast, the NO conversion profile of the 10 wt % CuO/γ-Al_2O_3 sample is peculiar: at ∼410 °C it drops to 0% and becomes negative at even higher temperatures (reaches ∼−70% at 550 °C). The negative NO conversion observed over the 10 wt % CuO/γ-Al_2O_3 is a consequence of the extensive oxidation of NH_3 to NO_x at higher temperatures under the highly oxidizing conditions. Indeed, the results presented in Figure 1(b) clearly show that the amount of NO_2 produced under SCR conditions over the 10 wt % CuO/γ-Al_2O_3 sample increases dramatically above 350 °C, but it becomes measurable only above 500 °C for the 0.5 wt % CuO/γ-Al_2O_3 catalyst.

Due to the high CuO loading in the 10 wt % CuO/γ-Al_2O_3 catalyst, the presence of large CuO particles is expected. The reactivity profile of this sample strongly suggests that the large CuO clusters formed on the alumina surface are more effective for the oxidation of NH_3 to NO_x under lean conditions than the small, perhaps even "atomically dispersed" CuO centers present in the 0.5 wt % sample. Thus, the observed differences in NO reduction and NH_3 oxidation over these two catalysts suggest that there are likely to be different types of Cu-containing species present on the alumina support, depending on the Cu loading. More importantly, such different catalytic centers must be responsible for the high selectivities observed

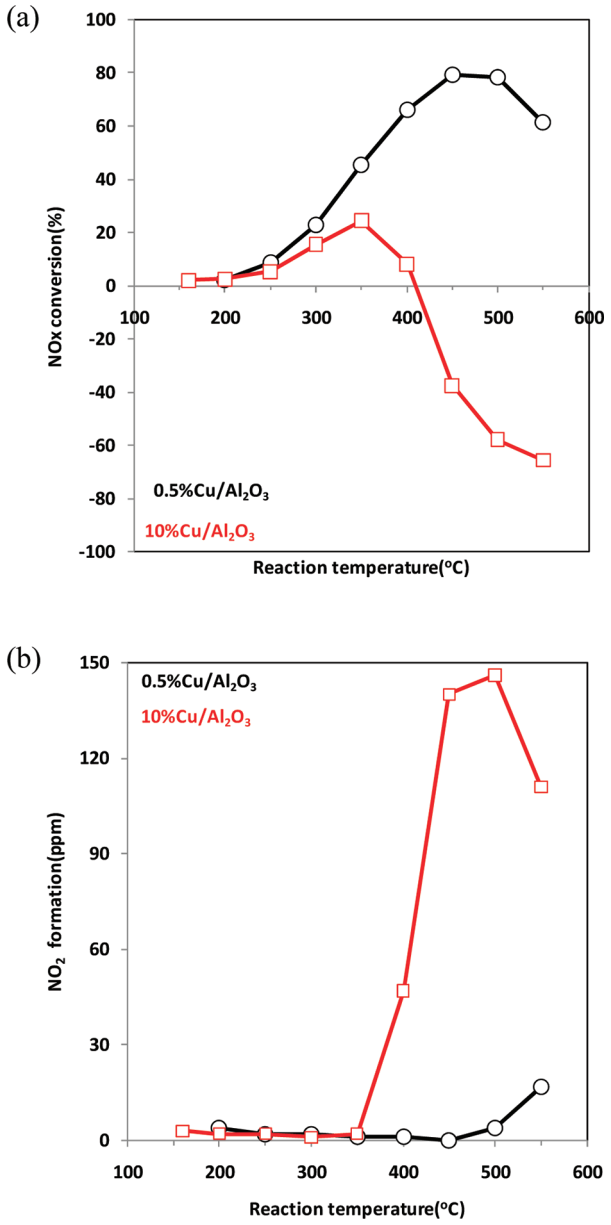

Figure 1. NO_x conversion (a) and NO_2 formation (b) profiles during the NH_3−SCR reaction on 10 wt % CuO/γ-Al_2O_3 (red) and 0.5 wt % CuO/γ-Al_2O_3 (black) catalysts.

toward either NO reduction (low CuO loading) or NH_3 oxidation (high CuO loading). (To compare selectivities obtained over the two catalysts, we have conducted catalytic measurements under conditions (i.e., different space velocities) where the NH_3 conversions over the two catalysts were very similar. The results of these measurements are displayed in the Supporting Information in Figures S1 and S2. Nearly overlapping NH_3 conversion profiles for the 0.5 wt % and 10 wt % CuO/γ-Al_2O_3 samples were obtained when the SCR reaction was carried out at 30 000 and 90 000 h^{-1} GHSVs, respectively. The NO_x-to-N_2 conversion profiles determined under these conditions and displayed in Figure S2 exhibit the same trends as we show in Figure 1a, although the absolute values somewhat differ because of the different reaction/analysis systems used in these two series of experiments.)

To gain further insight into the reactivity differences of the two catalysts discussed above, the oxidation of ammonia was

dx.doi.org/10.1021/cs3002463 | ACS Catal. 2012, 2, 1432−1440

separately examined under the same reaction conditions, but without NO in the reactant gas mixture. Under these conditions, NH_3 can be oxidized by O_2 to N_2, NO and NO_2. The results shown in Figure 2a demonstrate no NH_3 oxidation

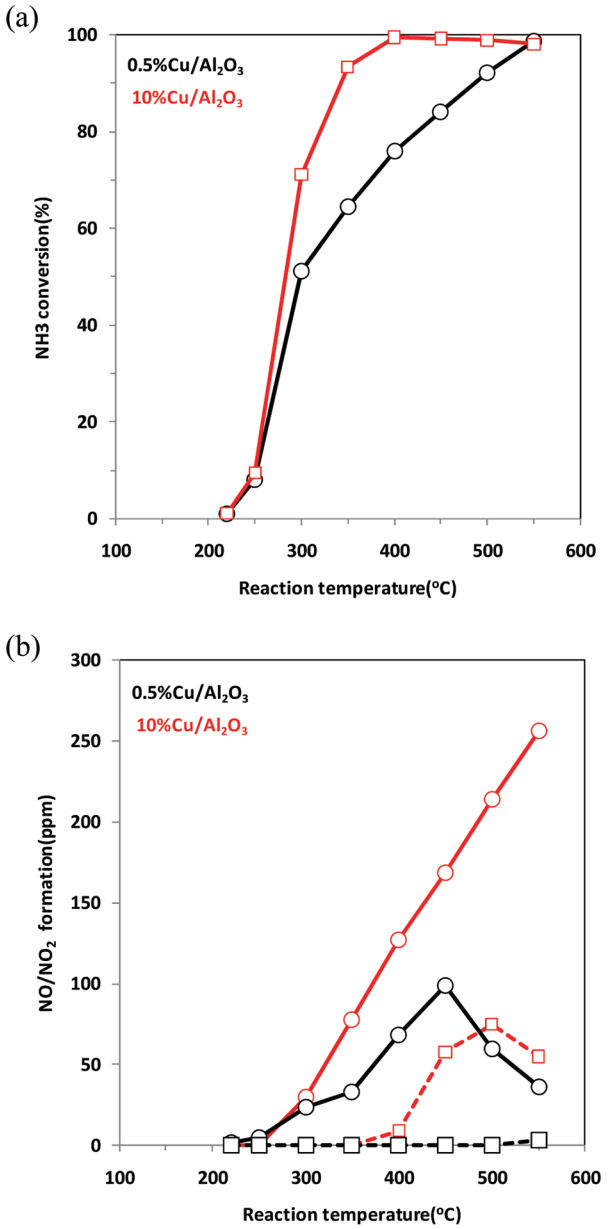

Figure 2. NH_3 conversion (a), and NO (solid line) and NO_2 (dotted line) formation (b) profiles during the NH_3 oxidation reaction on 10 wt % CuO/γ-Al_2O_3 (red) and 0.5 wt % CuO/γ-Al_2O_3 (black) catalysts.

activity over either catalyst below 200 °C, whereas above 220 °C, the NH_3 conversion increases rapidly for both catalysts. Comparing the NH_3 conversion profiles for the 0.5 wt % and 10 wt % CuO/γ-Al_2O_3 samples, we find significant differences: most importantly, the catalyst with high CuO loading is much more active for ammonia oxidation than the one with low CuO loading. In fact, the NH_3 conversion over the 10 wt % CuO/Al_2O_3 catalyst reaches 100% at 200 °C lower reactor temperature than the 0.5 wt % CuO/γ-Al_2O_3 sample. The amounts of NO and NO_2 formed in the NH_3 oxidation reaction over the two catalysts are displayed in Figure 2b.

In addition to the large amount of NO formed over the 10 wt % CuO/γ-Al_2O_3 catalyst, NO_2 was also produced in significant quantities, mainly at temperatures above 350 °C. On the other hand, only a trace amount of NO_2 was detected from the reaction over the 0.5 wt % CuO/γ-Al_2O_3 sample at the highest temperature studied. These differences between the two catalysts studied underline again the much higher ammonia oxidation activity of the 10 wt % CuO/Al_2O_3 in comparison with 0.5 wt % CuO/γ-Al_2O_3. The observed very high NH_3 oxidation activity of the highly CuO-loaded sample strongly reduces the amount of NH_3 available for NO reduction in the SCR gas mixture and, at the same time, increases the overall NO_x concentration. In contrast, much lower rates of NH_3 oxidation by O_2 over the 0.5 wt % CuO/γ-Al_2O_3 catalyst means that more ammonia will be available for the reduction of NO. The nitrogen balance also indicates that most of the NO_x initially produced from the oxidation of NH_3 over the 0.5 wt % CuO/γ-Al_2O_3 was subsequently consumed by NH_3 (still present in substantial concentration) through the SCR reaction.

3.2. H_2-TPR. To understand the nature of CuO in alumina-supported catalysts, we performed H_2-TPR experiments on the 0.5 wt % and 10 wt % Cu-loaded catalysts discussed above, and the results are shown in Figure 3. The H_2-TPR profile obtained

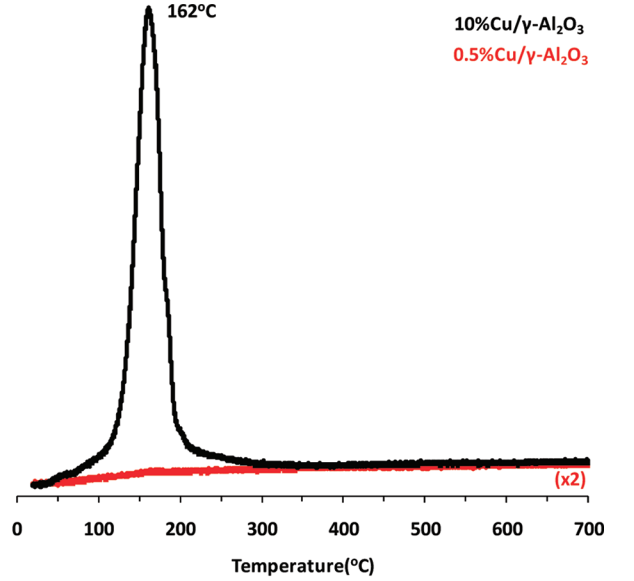

Figure 3. H_2-TPR on 10 wt % CuO/Al_2O_3 (black, using 50 mg of catalyst) and 0.5 wt % CuO/γ-Al_2O_3 (red, 100 mg).

from the 10 wt % CuO/γ-Al_2O_3 sample shows a sharp, symmetric peak centered at ~160 °C and a small feature at ~215 °C. The amount of hydrogen consumed was quantified on the basis of the results obtained from a CuO/SiO_2 standard, which showed one H_2 consumption peak at ~230 °C (in this standard sample, the H_2/Cu ratio is equal to 1 because the CuO is completely reduced to metallic Cu). This quantification provided a H_2/Cu value of ~0.62, indicating that ~40% of Cu loaded onto the alumina support was not reduced under the conditions of our TPR experiment. Even more interesting is the H_2-TPR profile measured from the 0.5 wt % CuO/γ-Al_2O_3 catalyst: it showed essentially no H_2 consumption up to 700 °C. This latter result can be explained only if we assume that (a) the sample had already gone through complete reduction during purging with the H_2/Ar gas mixture at room

dx.doi.org/10.1021/cs3002463 | ACS Catal. 2012, 2, 1432–1440

temperature prior to the start of temperature ramping or (b) it cannot be reduced under the TPR conditions applied in this study. However, no noticeable change was observed in the color of either of the catalysts during H_2/Ar purging at 300 K before temperature ramping, strongly suggesting that the Cu species in the 0.5 wt % Cu/γ-Al_2O_3 sample were not reducible.

The formation of $CuAl_2O_4$ after high-temperature treatment of CuO/γ-Al_2O_3 has been reported previously, and it was shown not to exhibit any measurable reduction during H_2-TPR;[21] however, our TPR experiment performed on a commercial $CuAl_2O_4$ sample showed a broad reduction peak centered at 560 °C (data not shown for brevity). Furthermore, the quantification of the H_2 consumption suggests a complete reduction of Cu in $CuAl_2O_4$ because the H_2/Cu ratio was ~1. This result strongly suggests that the Cu-containing species present on the alumina support in our 0.5 wt % CuO/γ-Al_2O_3 sample is different from those in $CuAl_2O_4$. The results of the H_2-TPR experiments from these two CuO/γ-Al_2O_3 samples provide a strong argument for the reduction of the bridging oxygens (Cu−O−Cu) in CuO clusters. We propose that no oxygen bridging of Cu−O−Cu type is present in the 0.5 wt % Cu/γ-Al_2O_3 sample; therefore, no H_2 consumption peak is observed in the H_2-TPR experiment. More importantly, this would suggest the presence of primarily monomeric Cu species on the alumina surface at this low Cu loading.

We recently reported the formation of monomeric or dimeric PtO and BaO species on the alumina surface by ultrahigh magnetic field solid state ^{27}Al NMR and STEM supported by DFT simulation. These studies clearly demonstrated the presence of a specific interaction between oxides and coordinatively unsaturated sites (pentacoordinate Al^{3+}) formed on the (100) facets of γ-alumina.[7−9] We propose that similar, highly dispersed surface species (i.e., monomeric CuO) are formed on the alumina surfaces in the 0.5 wt % CuO/γ-Al_2O_3 catalyst. Assuming that most of the Cu ions are present on the alumina surface as monomeric (CuO) units and that Cu is anchored to the support surface through an oxygen bridge (i.e., Cu−O−Al), H_2 consumption during TPR would arise from the removal of these bridging oxygen atoms. The results obtained indicate that the removal of this oxygen by reduction with H_2 is rather difficult and does not take place under the conditions applied in this study. On the contrary, the bridging oxygens in the CuO clusters can readily be reduced, resulting in a TPR peak at ~160 °C for the 10 wt % CuO/γ-Al_2O_3 catalyst. The totally different reducibility of CuO in these two extreme cases may help to explain the significantly different SCR performances discussed above for the 0.5 and 10 wt % CuO/γ-Al_2O_3 catalysts.

3.3. Catalyst Characterization by TEM and EXAFS. In the previous sections, we have established that the chemical properties (both the catalytic reaction pathways and reducibilities) of CuO species were fundamentally different when CuO was present in high dispersion (presumably in atomic dispersion) and in clusters or rafts. To learn about the dispersion of the CuO species on the alumina, microscopy and spectroscopy (STEM and EXAFS) studies were carried out on the CuO/γ-Al_2O_3 catalysts. STEM images collected from the 0.5 wt % and 10 wt % CuO/γ-Al_2O_3 samples after calcination at 500 °C are shown in Figure 4. The images from the 10 wt % CuO/Al_2O_3 catalyst (Figure 4a, b) clearly show the presence of CuO nanoparticles (~2 nm) on the alumina surface. In contrast, no distinguishable features that would suggest the presence of CuO clusters are observed in the STEM images

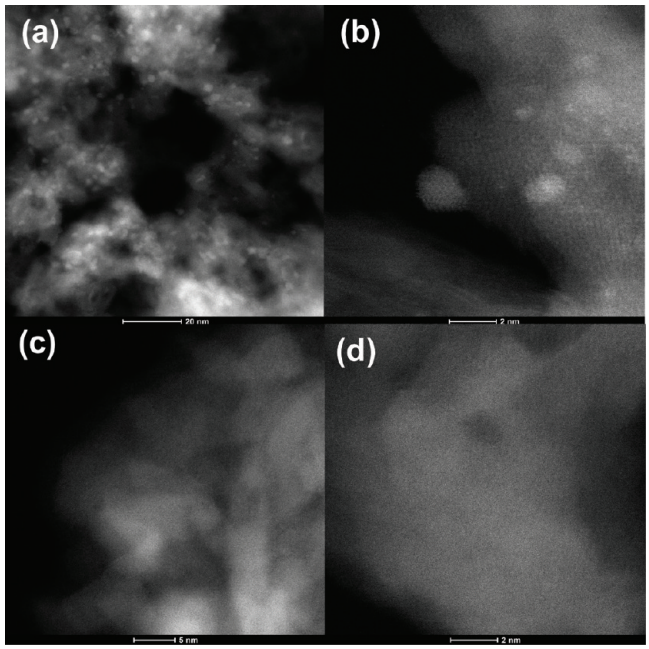

Figure 4. STEM images of 10 wt % CuO/γ-Al_2O_3 (a,b) and 0.5 wt % CuO/γ-Al_2O_3 (c,d) after calcination at 500 °C.

collected from the 0.5 wt % CuO/γ-Al_2O_3 sample (Figure 4c, d). The fact that no CuO nanoparticles could be identified in the images of the 0.5 wt % CuO/γ-Al_2O_3 sample provides strong evidence for the formation of highly dispersed CuO species, possibly in monoatomic form. Such highly dispersed species can routinely be resolved for higher Z elements with aberration-corrected microscopy.[22] However, because of both the relatively small difference in the atomic weight between Al (at. wt 27) and Cu (at. wt 63.5) (i.e., low Z contrast) and the presence of relatively thick alumina crystallites, the detection of atomically dispersed copper was not possible with the microscope available for this work.

Since STEM results could not unambiguously substantiate the presence of a monoatomic copper distribution in the 0.5 wt % CuO/γ-Al_2O_3 catalyst, we conducted EXAFS measurements on three catalysts and attempted to identify the neighboring atoms around the Cu scatterers, especially in the second coordination sphere. Before discussing the results we obtained in this study, we need to mention that, despite our efforts to analyze the 0.5 wt % CuO/γ-Al_2O_3 sample, because of its low Cu content, we could not obtain data with high enough quality that would have provided detailed structural information for this material. Therefore, conclusions on the structure of the 0.5 wt % CuO/γ-Al_2O_3 sample are made by extrapolating from the results obtained on 2, 5, and 10 wt % CuO/γ-Al_2O_3 samples. Figure 5 shows the derivative of normalized Cu K-edge X-ray absorption spectra for a number of Cu-containing samples (CuO (a), $CuAl_2O_4$ (b), and CuO (2 wt %, c; 5 wt %, d; and 10 wt %, e)/γ-Al_2O_3). The absorption energy was set to ~8990 eV, where the inflection point was zero, because the near-edge region was complicated as a result of the presence of multiple scattering features. The X-ray absorption near edge did not change significantly with the increase in Cu loading on γ-Al_2O_3. As shown in Figure 5, the XANES spectrum of the bulk $CuAl_2O_4$ was similar to those of CuO/γ-Al_2O_3, and the bulk CuO resulted in somewhat different spectra. Thus, these comparative XANES spectra indicate that the copper-

dx.doi.org/10.1021/cs3002463 | ACS Catal. 2012, 2, 1432−1440

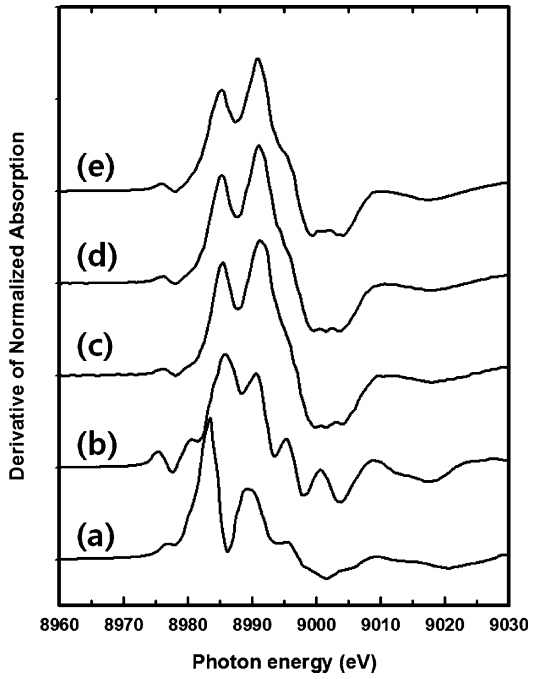

Figure 5. The derivative of the normalized X-ray absorption as a function of photon energy: (a) bulk CuO, (b) bulk $CuAl_2O_4$, (c) 2 wt % CuO/γ-Al_2O_3, (d) 5 wt % CuO/γ-Al_2O_3, and (e) 10 wt % CuO/Al_2O_3.

containing species on the alumina support resemble those present in $CuAl_2O_4$ rather than those in CuO.

The Fourier transform of Cu K edge EXAFS data after k^3 weighting and phase-shift correction with respect to the Cu−O bond are displayed in Figure 6 for CuO (a), $CuAl_2O_4$ (b), and 10 wt % CuO/γ-Al_2O_3 (c). The best fit to the function is also shown as blue dashed lines in Figure 6c for 10 wt % CuO/γ-Al_2O_3. The fitting was started with the theoretical $CuAl_2O_4$ standard. Comparison of the experimental radial distribution function with the theoretical radial distribution function

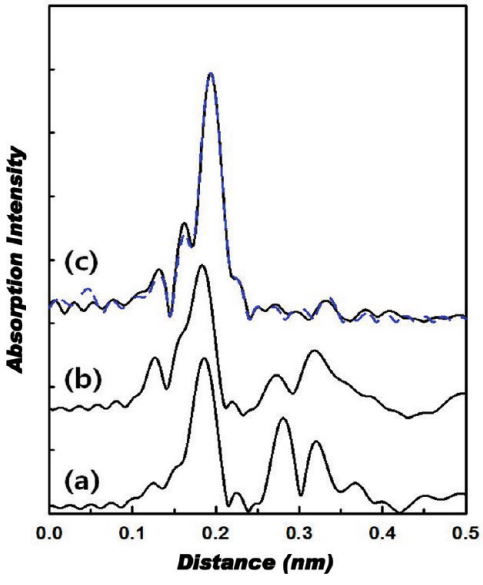

Figure 6. The phase shift-corrected Fourier transformation of k^3-weighted $\chi(k)$ spectra (solid lines) and the best fit function (blue dashed line): (a) CuO, (b) $CuAl_2O_4$, and (c) 10 wt % CuO/γ-Al_2O_3.

generated from *Feff6* suggested that the first peak at 0.2 nm arises from Cu−O nearest-neighbor scattering, whereas the second peak at 0.345 nm in the 10 wt % CuO/γ-Al_2O_3 sample corresponds to Cu−Cu(Al) scattering. Further comparison with the experimental reference spectra indicate that the Cu species in this sample is $CuAl_2O_4$-like. We found hardly any scattering related Cu−Cu(Al) on 2 wt % and 5 wt % CuO/γ-Al_2O_3 samples, most probably a result of the much higher dispersion of the Cu-containing phase at these loadings. This result supports the highly (atomically) dispersed CuO formation on 0.5 wt % CuO/γ-Al_2O_3, even though we could not get a high-quality EXAFS data for detailed analysis on this sample due to low Cu loading.

The experimental spectra were fit with multishells of *Feff6* scattering path extending up to 0.36 nm. The Nyquist theorem indicates that there are 19 independent data points within the given data range, Δk = 20−150 nm^{-1} and Δr = 0.13−0.36 nm.[10,11] In the curve-fitting, only eight variables, including ΔE_0 shift for each path, were used rigorously. As shown in Figure 6, the fitting quality was good and consistent. The structural parameters obtained from these fits are listed in Table 1. The first shell, consisting of 3−4 oxygen atoms at 0.195 nm, was evident in all samples. However, the second shell at 0.35 nm was significant only in the 10 wt % CuO/γ-Al_2O_3 sample. Furthermore, the coordination number corresponding to Cu−Cu(Al) in this latter sample was ∼1.7, indicating the presence of raft-like CuO species dispersed on γ-Al_2O_3. The conclusion we can draw from these XANES and EXAFS results is that high dispersions of Cu oxide were obtained, even at 10 wt % Cu loading. Furthermore, the absence of Cu in the second neighbor coordination in the 2 and 5 wt % CuO/γ-Al_2O_3 samples suggests very high dispersion of the CuO phase in these catalysts. Extrapolating from these results, we can conclude with high confidence that, in the 0.5 wt % CuO/γ-Al_2O_3 sample, the active catalytic phase is monoatomically dispersed on the alumina support.

3.4. DFT Calculations. On the basis of our previous experimental and theoretical work,[8,9,23−26] the penta-coordinated Al_V sites, which are only present on the (100) facets of γ-Al_2O_3, are the most likely nucleation sites for supported CuO particles on γ-Al_2O_3. As such, a periodic fully dehydrated γ-Al_2O_3(100)-(2 × 2) surface slab with eight atomic layers was used to represent the γ-Al_2O_3 substrate in the present study. This model γ-Al_2O_3(100) surface with 4 units of Al_2O_3 has also been extensively used and justified in our previous DFT studies of BaO/γ-Al_2O_3 and PtO/γ-Al_2O_3 systems.[8,9,23−25]

To investigate morphology effects of supported CuO particles on the NO reduction kinetics, two model catalysts, γ-Al_2O_3(100)-supported CuO monomer (CuO/γ-Al_2O_3) and two-dimension (2D) CuO monolayer ($CuO_{monolayer}/\gamma$-Al_2O_3), were used to represent CuO/γ-Al_2O_3 catalysts with low (0.5 wt %) and high (10 wt %) loadings, respectively. For the 2D CuO monolayer, a stoichiometric cation−anion matching scheme was used. As a result, the 2D CuO monolayer consists of four units of Cu_3O_2. The Cu−O bond lengths calculated from DFT are in good agreement with the expereimental EXAFS results, that is, the calculated Cu−O bond lengths are 1.90 and 1.78 Å, which are close to the 1.94 Å measured from EXAFS results. DFT results suggest that the Cu−O bond length increases in the supported CuO monolayer, which is also consistent with EXAFS results in that the Cu−O bond length increases from 1.94 to 1.96 Å when the loading increases from 2 to 10 wt %.

dx.doi.org/10.1021/cs3002463 | *ACS Catal.* 2012, 2, 1432−1440

Table 1. Result of Multishell EXAFS Curve-Fitting of CuO/Al_2O_3 Catalysts

sample	pair	R (nm)	N	σ^2 (pm^2)	R factor
2 wt % CuO/γ-Al_2O_3	Cu−O	0.1947 (0.0006)	3.5 (0.3)	44 (8)	0.00016
	Cu−Cu(Al)				
5 wt % CuO/γ-Al_2O_3	Cu−O	0.1946 (0.0005)	3.3 (0.2)	45 (6)	0.00009
	Cu−Cu(Al)				
10 wt % CuO/γ-Al_2O_3	Cu−O	0.1961 (0.0007)	3.3 (0.3)	48 (6)	0.00079
	Cu−Cu(Al)[a]	0.3508 (0.0056)	1.7 (1.3)	94 (54)	

[a]Cu−Cu(Al) contribution can be regarded as Cu−O−Cu(Al).

The interaction of NO and O_2 and their activation reactions on both model catalyst surfaces were studied. The adsorption energies of NO and O_2 on the CuO/γ-Al_2O_3 and $CuO_{monolayer}/\gamma$-Al_2O_3 were calculated as follows:

$$E_{ad} = E_{adsorbate+surface} - (E_{surface} + E_{adsorbate}) \quad (1)$$

where $E_{adsorbate+surface}$ is the total energy of the interacting system of the surface slab (CuO/γ-Al_2O_3 or $CuO_{monolayer}/\gamma$-Al_2O_3) and the adsorbed NO or O_2, $E_{surface}$ is the total energy of the optimized bare CuO/γ-Al_2O_3 and $CuO_{monolayer}/\gamma$-Al_2O_3 surface slabs, and $E_{adsorbate}$ is the energy of isolated NO or O_2 (in the triplet state) molecules in vacuum. For species such as atomic N + O and O + O from NO and O_2 dissociation, respectively, the calculated adsorption energies are also referred to isolated NO and O_2 molecular energies in vacuum. On the basis of this definition, a negative E_{ad} value indicates favorable (exothermic) adsorption.

Before studying the morphological effects of supported CuO on NO and O_2 activation, we first examined the structures and interactions of a CuO monomeric unit and CuO monolayer on the fully dehydrated γ-Al_2O_3 (100) surface. The optimized structures of these two model surfaces are shown in Figure 7.

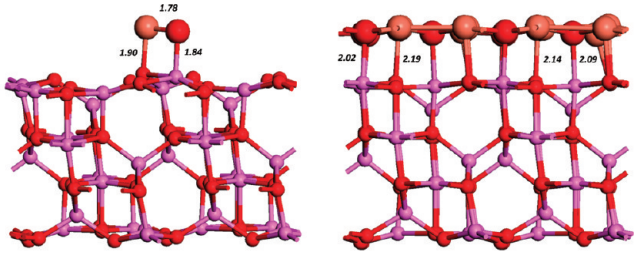

Figure 7. Side views of optimized structures of a CuO monomer (a) and a CuO monolayer (Cu_8O_{12}) (b) on the fully dehydrated γ-Al_2O_3(100) surfaces. Al atoms are in magenta; O atoms are in red; and Cu atoms are in pink. The numbers shown in the figure are bond lengths in Å.

For the CuO/γ-Al_2O_3 surface, the bond lengths of Cu−O_s (O_s denotes an alumina surface O atom), Al−O, and Cu−O are 1.90, 1.84, and 1.78 Å, respectively. Referenced to the gas-phase CuO monomer, the binding interaction between the monomeric CuO and the γ-Al_2O_3 substrate is 1.84 eV. For the $CuO_{monolayer}/\gamma$-Al_2O_3 surface, the bond lengths of Cu−O_s and Al−O are slightly increased. The calculated interaction between the 2D CuO monolayer and the γ-Al_2O_3 substrate is 5.18 eV.

To elucidate distinguishable NO reduction kinetics that are associated with different Cu loadings, we calculated adsorption and dissociation reactions of NO and O_2 on both CuO/γ-Al_2O_3 and $CuO_{monolayer}/\gamma$-Al_2O_3 surfaces. The calculated adsorption energies of NO and O_2, along with their dissociation products (N + O, O + O) on the CuO/γ-Al_2O_3 and $CuO_{monolayer}/\gamma$-Al_2O_3 surfaces are given in Table 2. Various adsorption

Table 2. DFT Calculated Adsorption Energies, E_{ad} (in eV), of NO, O_2, Coadsorbed N and O atoms (N + O), and Coadsorbed O Atoms (O+O) on the $CuO_{monomer}/\gamma$-Al_2O_3 and $CuO_{monolayer}/\gamma$-Al_2O_3 Surfaces

	E_{ad}	
species	$CuO_{monomer}/\gamma$-Al_2O_3(100)	$CuO_{monolayer}/\gamma$-Al_2O_3(100)
NO	−1.25 (N and O both bound with Cu)	−2.35
	−0.86 (O bound with Cu)	
	−2.07 (N bound with Cu)	
N + O	+3.45	−2.28
O_2	−1.24	−1.77
O + O	+0.87	−1.15

configurations for NO, O_2, N + O, and O + O were examined. Figure 8 shows optimized structures of NO, N + O, O_2 and O

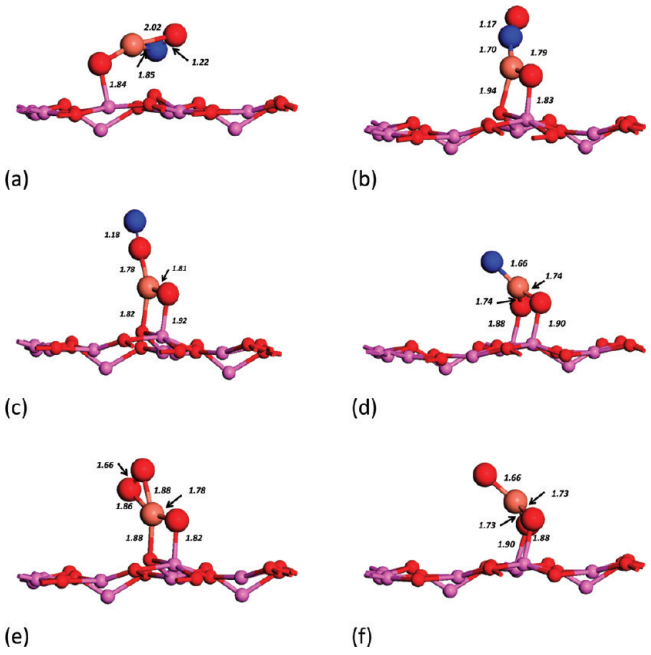

Figure 8. Side views of adsorbed NO and O_2, and their dissociation products on the CuO/γ-Al_2O_3 (100) surface. (a−c) Three stable configurations of adsorbed NO, (d) N + O, (e) O_2, and (f) O + O. The numbers shown in the figure are bond lengths in angstroms. Color scheme is the same as that used in Figure 8. The N atom is in blue.

dx.doi.org/10.1021/cs3002463 | ACS Catal. 2012, 2, 1432−1440

+ O on the CuO/γ-Al_2O_3 surface in their most stable configurations. As seen from Table 2, both NO and O_2 molecules bind with the supported isolated CuO monomer with nearly the same adsorption energies (−1.25 and −1.24 eV); however, our DFT results show that both NO and O_2 dissociation processes are highly endothermic (+4.6 and +2.1 eV) on the CuO/γ-Al_2O_3 surface, and thus, neither NO or O_2 will dissociate on the CuO/γ-Al_2O_3 surface. On the $CuO_{monolayer}$/γ-Al_2O_3 surface, both NO and O_2 adsorption energies are stronger (−2.35 and −1.77 eV, respectively). Furthermore, in this case, we find that the dissociation reactions of both NO and O_2 leading to N + O and O + O are only slightly endothermic (+0.07 and +0.32 eV). The calculated dissociation barriers for NO (Figure 9a) and O_2 (Figure 9c), forming N + O (Figure 9b) and O + O (Figure 9d), are 1.17 and 0.46 eV, indicating that dissociation of both NO and O_2 are feasible on the $CuO_{monolayer}$/γ-Al_2O_3 surface. Consequently, the formed reactive atomic oxygen is available for the oxidation of ammonia to generate NO_x. The contrasting unavailability of atomic oxygen species from either NO or O_2 dissociation on the monomeric CuO/γ-Al_2O_3 surface may explain enhanced selectivity to an N_2 product from a reaction with molecularly adsorbed NO with NH_3 for this catalyst.

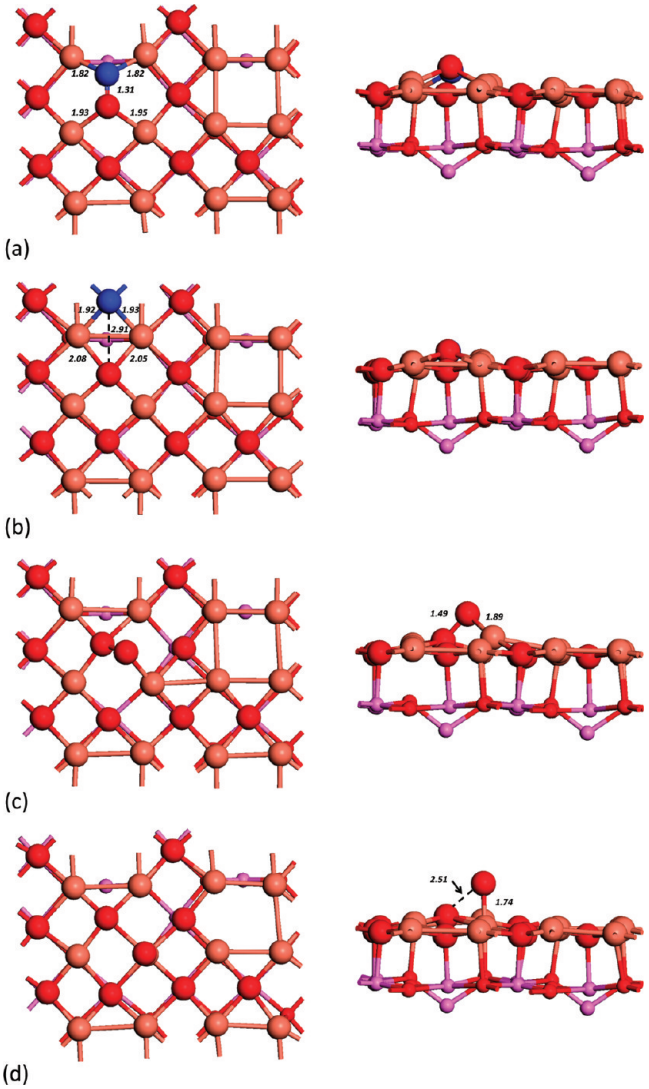

Figure 9. Top and side views of adsorbed NO and O_2 and dissociation products on the $CuO_{monolayer}$/γ-Al_2O_3 (100) surface. The figures on the left are the top views; the figures on the right are the side views. (a) NO, (b) N + O, (c) O_2, and (d) O + O. The numbers shown in the figure are bond lengths in angstroms. Color scheme is the same used in Figures 7 and 8.

One interesting point we should mention here is the similarity of the NH_3 SCR reaction over low-loaded CuO/Al_2O_3 and well-known Cu-zeolite catalysts. Although the environments around the active catalytic centers in these two catalyst systems are significantly different, isolated Cu species are likely present in both catalysts, and these structures may be the active sites for the NH_3 SCR reaction.[27]

4. CONCLUSIONS

Catalytic reaction pathways of NH_3 on γ-Al_2O_3-supported Cu catalysts during NH_3 SCR reactions under lean conditions were investigated. On 10 wt % CuO/γ-Al_2O_3, NH_3 reacts primarily with oxygen to produce NO_x. However, on a 0.5 wt % CuO/γ-Al_2O_3 catalyst, NH_3 reacts with NO to form N_2, and the NO_x conversion to N_2 was almost 80% at 450 °C. H_2-TPR results show that Cu species present in the 10 wt % CuO/γ-Al_2O_3 catalyst are readily reducible, and a H_2 consumption peak at ∼160 °C strongly suggests the formation of large CuO clusters on the alumina surface. However, the TPR spectrum obtained from the 0.5 wt % CuO/γ-Al_2O_3 catalyst shows little, if any, H_2 consumption up to 700 °C, strongly suggesting the presence of isolated and, thus, nonreducible Cu species. STEM images collected from 10 wt % CuO/γ-Al_2O_3 catalyst show nanosized CuO clusters, but no evidence of Cu on the 0.5 wt % CuO/γ-Al_2O_3 sample is seen because of the low Z contrast between very highly dispersed Cu species and the alumina support material. EXAFS data show Cu−Cu(Al) coordination in the second shell at 0.35 nm only in the 10 wt % CuO/γ-Al_2O_3 sample, with a coordination number estimated to be ∼1.7. The XANES and EXAFS results confirm the presence of highly dispersed Cu oxide, even at 10 wt % CuO loading, indirectly suggesting a much higher, even atomic copper dispersion in the 0.5 wt % Cu-containing sample. DFT calculations show that γ-Al_2O_3-supported 2D CuO clusters (rafts) can strongly interact with both adsorbed NO and O_2 and that dissociation of these species is relatively facile. The thus formed atomic oxygen species in the 10 wt % CuO/γ-Al_2O_3 catalyst may be responsible for producing NO_x via the oxidation of ammonia. In contrast, supported monomeric CuO units are not able to break the N−O or O−O bonds due to the high endothermicities of these processes. As such, instead of generating NO_x, as in the case for the supported 2D CuO clusters with high CuO loading, molecularly adsorbed NO reacts with NH_3 to produce N_2 over γ-Al_2O_3-supported isolated monomeric CuO.

■ ASSOCIATED CONTENT

Supporting Information

NH_3 and NO_x conversion profiles obtained at 30 000 and 90 000 h^{-1} GHSVs for the 0.5 wt % and 10 wt % CuO/γ-Al_2O_3 samples are shown in Figures S1 and S2, respectively. This material is available free of charge via the Internet at http://pubs.acs.org.

dx.doi.org/10.1021/cs3002463 | ACS Catal. 2012, 2, 1432−1440

AUTHOR INFORMATION

Corresponding Author

*E-mails: (J.H.K.) kwak@pnnl.gov, (D.M.) donghai.mei@pnnl.gov.

Notes

The authors declare no competing financial interest.

ACKNOWLEDGMENTS

We gratefully acknowledge the US Department of Energy (DOE), Office of Basic Energy Sciences, Division of Chemical Sciences, and the DOE's Office of Vehicle Technologies for the support of this work. D. Mei is supported by the Laboratory Directed Research and Development (LDRD) project at Pacific Northwest National Laboratory (PNNL). PNNL is operated for the US DOE by Battelle Memorial Institute under contract number DE-AC05-76RL01830. The research described in this paper was performed in the Environmental Molecular Sciences Laboratory (EMSL), a national scientific user facility sponsored by the DOE Office of Biological and Environmental Research and located at PNNL. Computing time was granted by a user project (st30469) at the Molecular Science Computing Facility in EMSL. The EXAFS data were collected using the National Synchrotron Light Source (NSLS) at Brookhaven National Laboratory; the NSLS is supported by the DOE, Office of Science/Basic Energy Sciences, under Contract No. DE-AC02-98CH10886.

REFERENCES

(1) Bell, A. T. *Science* **2003**, *299*, 1688.
(2) Tauster, S. J.; Fung, S. C.; Baker, R. T. K.; Horsley, J. A. *Science* **1981**, *211*, 1121.
(3) Kulkarni, A.; Chi, M. F.; Ortalan, V.; Browning, N. D.; Gates, B. C. *Angew. Chem., Int. Ed.* **2010**, *49*, 10089.
(4) Nellist, P. D.; Pennycook, S. J. *Science* **1996**, *274*, 413.
(5) Chen, M. S.; Goodman, D. W. *Science* **2004**, *306*, 252.
(6) Lei, Y.; Mehmood, F.; Lee, S.; Greeley, J.; Lee, B.; Seifert, S.; Winans, R. E.; Elam, J. W.; Meyer, R. J.; Redfern, P. C.; Teschner, D.; Schlogl, R.; Pellin, M. J.; Curtiss, L. A.; Vajda, S. *Science* **2010**, *328*, 224.
(7) Kwak, J. H.; Hu, J. Z.; Kim, D. H.; Szanyi, J.; Peden, C. H. F. *J. Catal.* **2007**, *251*, 189.
(8) Kwak, J. H.; Hu, J. Z.; Mei, D.; Yi, C. W.; Kim, D. H.; Peden, C. H. F.; Allard, L. F.; Szanyi, J. *Science* **2009**, *325*, 1670.
(9) Kwak, J. H.; Mei, D. H.; Yi, C. W.; Kim, D. H.; Peden, C. H. F.; Allard, L. F.; Szanyi, J. *J. Catal.* **2009**, *261*, 17.
(10) Frenkel, A. I.; Stern, E. A.; Qian, M.; Newville, M. *Phys. Rev. B* **1993**, *48*, 12449.
(11) Newville, M.; Livins, P.; Yacoby, Y.; Rehr, J. J.; Stern, E. A. *Phys. Rev. B* **1993**, *47*, 14126.
(12) Kresse, G.; Furthmuller, J. *Phys. Rev. B* **1996**, *54*, 11169.
(13) Kresse, G.; Furthmuller, J. *Comput. Mater. Sci.* **1996**, *6*, 15.
(14) Kresse, G.; Hafner, J. *Phys. Rev. B* **1994**, *49*, 14251.
(15) Blochl, P. E. *Phys. Rev. B* **1994**, *50*, 17953.
(16) Kresse, G.; Joubert, D. *Phys. Rev. B* **1999**, *59*, 1758.
(17) Perdew, J. P.; Burke, K.; Ernzerhof, M. *Phys. Rev. Lett.* **1996**, *77*, 3865.
(18) Mills, G.; Jonsson, H.; Schenter, G. K. *Surf. Sci.* **1995**, *324*, 305.
(19) Henkelman, G.; Jonsson, H. *J. Chem. Phys.* **2000**, *113*, 9978.
(20) Henkelman, G.; Uberuaga, B. P.; Jonsson, H. *J. Chem. Phys.* **2000**, *113*, 9901.
(21) Yan, J. Y.; Lei, G. D.; Sachtler, W. M. H.; Kung, H. H. *J. Catal.* **1996**, *161*, 43.
(22) Hartel, P.; Rose, H.; Dinges, C. *Ultramicroscopy* **1996**, *63*, 93.
(23) Mei, D. H.; Kwak, J. H.; Szanyi, J.; Ge, Q. F.; Peden, C. H. F. *Catal. Today* **2010**, *151*, 304.
(24) Mei, D. H.; Kwak, J. H.; Hu, J. Z.; Cho, S. J.; Szanyi, J.; Allard, L. F.; Peden, C. H. F. *J. Phys. Chem. Lett.* **2010**, *1*, 2688.
(25) Mei, D. H.; Ge, Q. F.; Kwak, J. H.; Kim, D. H.; Verrier, C.; Szanyi, J.; Peden, C. H. F. *Phys. Chem. Chem. Phys.* **2009**, *11*, 3380.
(26) Mei, D.; Ge, Q. F.; Szanyi, J.; Peden, C. H. F. *J. Phys. Chem. C* **2009**, *113*, 7779.
(27) Iwamoto, M.; Yahiro, H.; Torikai, Y.; Yoshioka, T.; Mizuno, N. *Chem. Lett.* **1990**, 1967.